Chinese Journal of Structural Chemistry

ARTICLE

Interfacial Engineering of NiFeP/NiFe-LDH Heterojunction for Efficient Overall Water Splitting

Xuanyu Long[1], Jiazhi Meng[1], Jiabao Gu[1], Lanqing Ling[1], Qianwen Li[1], Nan Liu[1], Kaiwen Wang[2]* and Zequan Li[1]*

[1]*The School of Chemistry and Chemical Engineering, Chongqing University, Chongqing 400044, China*

[2]*Beijing Key Lab of Microstructure and Properties of Advanced Materials, Beijing University of Technology, Beijing 100124, China*

ABSTRACT In consideration of application prospect of non-noble metallic materials catalysts, the study of exploring more highly effective electrocatalysts has been focused on by researchers. Herein, a novel strategy is employed to construct a heterojunction consisting of metal phosphide Ni_xFe_yP and layered double hydroxide (LDH) with graphene oxide (GO) as conductive support. By adjusting the molar ratio of Ni to Fe, a series of heterojunctions with mixed valence state $Fe^{\delta+}/Fe^{3+}$ and $Ni^{\delta+}/Ni^{2+}$ (δ is likely close to 0) redox couples are achieved and strong synergistic effects towards overall water splitting performance are found. The optimized catalyst with a Ni/Fe molar ratio of 0.72:0.33, namely $Ni_{0.7}Fe_{0.3}P$/LDH/GO, delivers ultra-low overpotentials for hydrogen evolution reaction (HER) and oxygen evolution reaction (OER) of 79 and 198 mV at the current density of 10 $mA{\cdot}cm^{-2}$, respectively. Furthermore, for overall water-splitting practical application, it only requires 1.526 V at 10 $mA{\cdot}cm^{-2}$ with robust stability, which is superior to most reported electrocatalysts. Experimental results demonstrate the improved electronic conductivity, enlarged electrochemically active area and accelerated kinetics together account for the enhanced performance. This work supplies new prospects for the promotion and application of such heterojunction electrocatalysts in overall water splitting.

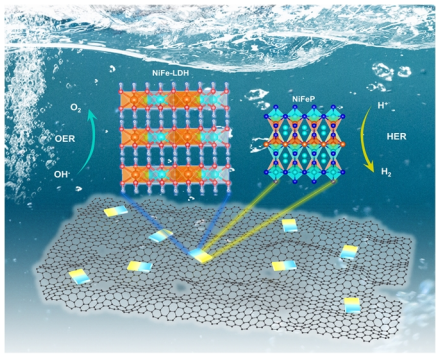

Keywords: overall water splitting, electrocatalysis, heterojunction, phosphide, layered double hydroxide

n INTRODUCTION

Electrochemical splitting of water into hydrogen and oxygen is expected as a sustainable technology for energy conversion and storage.[1] HER and OER are two half-reactions of the electrocatalytic water splitting, which is regarded as an important part of the "green" hydrogen production technology.[2-5] Even if their superb performance on water-splitting, noble metal-based catalysts, such as Pt, IrO_2, etc., are not sustainable catalysts due to their scarcity.[6,7] Consequently, developing electrocatalysts with lost cost and high activity is of vital necessity.[8] Among them, the transition metal phosphides (TMPs) have shown exceptional activity and durability towards HER, which is also proved by theoretical calculations.[9] For example, Ni_2P,[10] CoP[11] and Fe_2P[12] possess the advantages of controllable structures, adjustable electronic states, as well as excellent electrical conductivity, and subsequently outstanding HER performance. In these cases, the interaction between the 3*d* orbital of the transition metal and the 3*p* electrons of phosphorus facilitates the adsorption and desorption of the intermediates during HER.[9,13] However, in the matter of OER, due to its four-electron process property and multistep proton-coupled electron transfer (PCET), the kinetics is more sluggish than HER.[14] Recent studies have shown that the OER performance of transition metals layered-double hydroxides (TMs LDHs) can be comparable to that of IrO_2 due to their high specific surface area and unique layered structure.[15-18] Nevertheless, few LDHs themselves are ideal bifunctional electrocatalysts for overall water splitting. The exploitation of promising materials with simultaneously outstanding HER and OER activity is highly desired.

Interface engineering has been wildly used as an effective method to modify the electron states of electrocatalysts and modulate the adsorption-desorption properties of water-splitting intermediates, leading to adjustable electrocatalytic performance.[19,20] For instance, Meng *et al*. reported that the formation of $NiSe_2$-$CoSe_2$ hybrid structure would induce strong electronic effect and plenty of active high valence state metal species, exhibiting a low overpotential of 250 mV to reach 10 $mA{\cdot}cm^{-2}$.[21] Besides, the rational combining of the interface engineering and structural conductive substrates can also improve the performance. Recently, Paul K. Chu et al. have combined Mo_2C with VC to form a heterojunction and embedded itself into a graphitized carbon network structure, which improved the performance dramatically compared with single-component compound.[22] Li *et al.* reported a method where phosphorization and carbonization treatments were used to construct N-doped carbon supported CoP-WC heterojunction. As a result, the hydrogen evolution electrocatalyst performance greatly enhanced.[23] Constructing heterojunction with TMPs and LDH, the most promising candidates for HER and OER respectively, can achieve highly efficient dual-functional electrocatalytic water splitting. Furthermore, to enhance the stability of electrocatalysts, it is common to incorporate active materials with conductive substrates such as Ni foam[24] and graphene[25,26]. Inspired by the above strategies, it is promising to design an electrocatalyst with heterojunction consisting of TMPs and LDH attached tightly onto conductive materials.

Here, we synthesized a series of bimetallic heterojunctions constructed by Ni-Fe-P and Ni-Fe LDH via hydrothermal treatment and continuous in-situ phosphorization under Ar atmosphere. The

DOI: 10.14102/j.cnki.0254-5861.2022-0048

formed interface facilitates electron transfer and induces more active sites. Moreover, implying GO as substrate can not only promote electron transfer but hold the hererojunction tightly, effectively preventing the agglomeration of catalysts. Through adjusting the molar ratio of Ni to Fe in the as-made hybrids, improved kinetics property and electrochemically active area were achieved. The optimized $Ni_{0.7}Fe_{0.3}P$-LDH/GO delivered prominent HER and OER electrocatalytic activity which is comparable to that of state-of-the-art commercial Pt/C and IrO_2, respectively. Impressively, when applied into overall water splitting cell, the catalyst showed an ultralow voltage with 1.526 V at 10 mA·cm^{-2} and exhibited solid durability against fifty-hours running under work condition. The heterogeneous interface induced active site strategy would provide new possibilities for sustainable energy conversion and storage.

n RESULTS AND DISCUSSION

The synthetic process for the Ni_xFe_yP/LDH/GO is displayed in Figure 1a. Briefly, GO was fabricated by the modified Hummer method.[27]

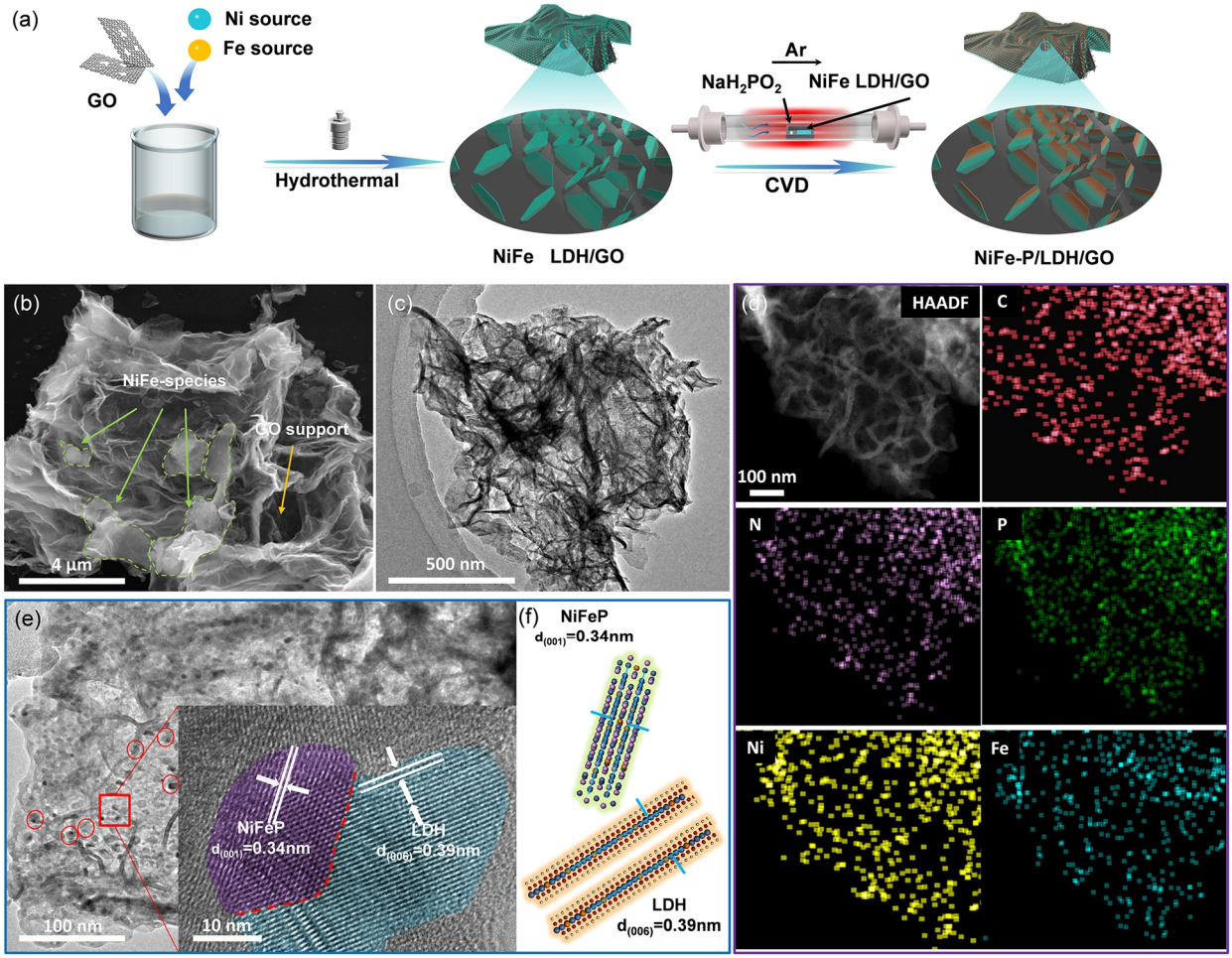

Figure 1. (a) Schematic illustration of the synthetic process for the Ni_xFe_yP/LDH/GO, (b) SEM image of $Ni_{0.7}Fe_{0.3}P$/LDH/GO, (c) low-magnification TEM of $Ni_{0.7}Fe_{0.3}P$/LDH/GO, (d) HAADF-STEM and elemental mapping of $Ni_{0.7}Fe_{0.3}P$/LDH/GO, (e) HRTEM of $Ni_{0.7}Fe_{0.3}P$/LDH/GO, (f) Schematic illustration of interface structure according to HRTEM results.

Subsequently, the obtained GO was assembled with different Ni/Fe molar ratios sources to form a GO supported bimetallic NiFe-LDH through hydrothermal reaction. Afterwards, in-situ transformation from NiFe-LDH to Ni_xFe_yP occurred under PH_3/Ar atmosphere, where PH_3 was released by NaH_2PO_2 pyrolysis.[28] According to this, Ni_xFe_yP/LDH/GO with different Ni/Fe molar ratios were synthesized as follows: $Ni_{0.5}Fe_{0.5}P$/LDH/GO, $Ni_{0.6}Fe_{0.4}P$/LDH/GO, $Ni_{0.7}Fe_{0.3}P$/LDH/GO and $Ni_{0.8}Fe_{0.2}P$/LDH/GO. As shown in Figure S1 and S2(a–d), the morphology of GO and GO/LDH was probed by scanning electron microscopy (SEM), confirming a folded two-dimensional GO supported nanosheets hybrid structure. Powder X-ray diffraction (XRD) was performed to verify their crystal structures (Figure S2e–f). A characteristic peak at 2θ≈9° corresponding to GO was observed.[25] The energy-dispersive X-ray spectroscopy (EDX, Figure S3) mapping clearly demonstrated homogeneous distribution of Ni, Fe, and O. Similarly, the morphology and element composition distribution of samples after phosphating treatment were studied by scanning electron microscope (SEM) (Figure 1b, S4), low-magnification transmission electron microscopy (Figure 1c), and EDX mapping (Figure 1d, S5). The

Chin. J. Struct. Chem. **2022**, 41, 2204046-2204053
DOI: 10.14102/j.cnki.0254-5861.2022-0048

overall morphology remains unchanged except that some smaller and brighter layered materials appear on GO. The EDX results also confirmed the successful introduction of P element. The interface between $Ni_{0.7}Fe_{0.3}P$ and LDH was further clarified via high-magnification TEM (Figure 1e), indicating two lattice fringes of 0.39 and 0.34 nm corresponding to LDH (006) plane[29] and the (001) plane[30] of NiFeP. The possible interface model according to HRTEM results is proposed in Figure 1f. To verify precise Ni/Fe molar ratio of designed Ni_xFe_yP/LDH/GO, ICP-MS was performed (Table S1). The results show that the Ni/Fe molar ratios of the as-made bimetal-induced heterojunction samples are 0.81:0.23, 0.72:0.33, 0.59:0.37 and 0.5:0.5, respectively. For simplicity, these samples are denoted as $Ni_{0.8}Fe_{0.2}P$/LDH/GO, $Ni_{0.7}Fe_{0.3}P$/LDH/GO and $Ni_{0.6}Fe_{0.4}P$/LDH/GO and $Ni_{0.5}Fe_{0.5}P$/LDH/GO. Notably, the atomic fraction of P decreased drastically after chemical etching (Table S2), instead of decreasing to the same degree as that of Ni and Fe when NiFe/LDH/GO was phosphatized thoroughly, which indicates that the bimetal-induced heterojunction is constructed.

The crystal structures of the samples were characterized by X-ray diffraction (Figure 2a, b). The peaks are indexed to LDH (JCPDS#00-040-0215), GO and Ni_xFe_yP (Ni_2P JCPDS#03-065-9706, Fe_2P JCPDS#01-083-2337). As shown in Figure 2b, with the variation of Ni/Fe molar ratio, the sharp peaks shift between pure phase Ni_2P and Fe_2P, which indicates atomic doping nature

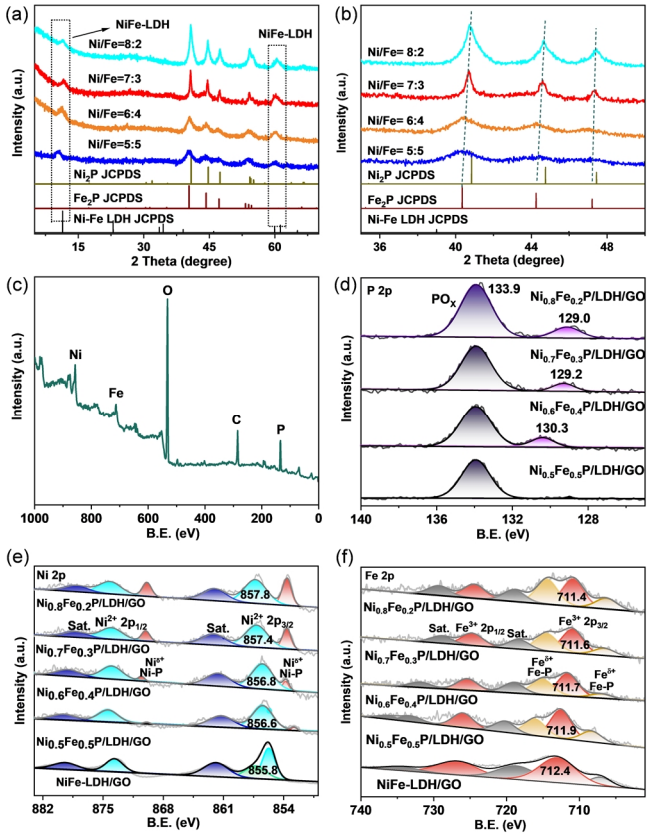

Figure 2. The structural characterization patterns of Ni_xFe_yP/LDH/GO with different Ni/Fe molar (a–b) XRD, (c–f) XPS, (c) XPS survey, (d) P 2*p*, (e) Ni 2*p*, (f) Fe 2*p* core levels.

of Ni and Fe. XPS analyses were carried out to study the surface chemical composition and electronic state of the Ni_xFe_yP/LDH/GO (Figure 2c–f). The peaks of Ni 2*p* in Figure 2e correspond to Ni $2p_{3/2}$ (853.6 and 856.6 eV) and Ni $2p_{1/2}$ (871.3 and 874.4 eV), consistent with reported nickel phosphide in the literature.[31] Particularly, a characteristic peak (853.2 eV) is found between Ni^{2+} $2p_{3/2}$ (853.6 eV) and metallic Ni (852.6 eV), which can be ascribed to phosphatized partially positive Ni species ($Ni^{\delta+}$, δ is close to 0) and assigned to the Ni–P bond.[32] The other peaks are ascribed to satellite peaks in Ni 2*p*.[32] In the Fe 2*p* spectrum (Figure 2f), the peaks around 711.2 and 725.4 eV in the Fe 2*p* high-resolution XPS spectrum represent Fe $2p_{3/2}$ and Fe $2p_{1/2}$, and correspond to Fe^{3+}.[8] The peaks positioned at 707.2 eV are between Fe^{3+} $2p_{3/2}$ (711.2 eV) and metallic Fe (706.8 eV), ascribed to altered partially positive Fe species ($Fe^{\delta+}$, δ is close to 0).[15] The peak at 716.1 eV is assigned to Fe–P bond.[12,34] Compared with LDH/GO, the emerging of Ni–P and Fe–P bonds further confirms the P incorporation into NiFe-LDH. In the high-resolution P 2*p* spectrum (Figure 2d), the peaks of P $2p_{3/2}$ (130.3 eV) and phosphate (133.9 eV) in Ni_xFe_yP/LDH/GO were detected.[35] Throughout Ni_xFe_yP/LDH/ GO samples, the XPS peaks of Ni, Fe and P elements shift obviously with the variation of Ni/Fe molar ratio, which indicates strong electronic coupling effect in the heterojunction.[36,37] By tailoring the Ni/Fe molar ratio, the interaction between Ni_xFe_yP and LDH can be modified and could bring about distinct change of the local electric dipole.[35] The characteristic peaks of C 1*s* and O 2*p* (Figure S6a–b) suggest the coexistence of C=C, C=O, O–C=O, Ni/Fe–O and O–H.[11,38,39] To further confirm the formation of Ni_xFe_yP and LDH heterojunction, thermogravimetric test was performed (Figure S7). TG analysis results show that the sample weight loss process could be identified as three stages. The first one is water loss from the LDH interlayer and adsorbs water molecules at 300 ℃, the second is the elimination of GO and the LDH interlayer carbonate anions between 300 and 600 ℃, and the last is the oxidation of Ni_xFe_yP above 600 ℃ as the temperature increased.[40,41]

To explore the influence of the Ni/Fe molar ratio on electrolyzed water, a three-electrode system was used to test their HER performance in 1 M KOH electrolyte (pH = 14). The prepared samples were coated on Ni foam (1×1 cm^2) to serve as the working electrode. In comparison to the performance of Ni_xFe_yP/ LDH/GO, Pt/C, LDH/GO and Ni foam were tested under the same conditions. LSV polarization curves were carried out to study HER performance (Figure 3a). The performance of Ni foam and LDH/GO is clearly inferior to that of Ni_xFe_yP/LDH/GO. The lowest value of Tafel slope for as-synthesized materials is 61 mV·decade^{-1} that belongs to $Ni_{0.7}Fe_{0.3}P$/LDH/GO in Figure 3b. Notably, after combining Ni_xFe_yP with LDH/GO, the electrocatalytic properties were enhanced in Figure 3c, which was evidenced by a close overpotential (79 mV) to Pt/C at 10 mA·cm^{-2} (20 = 110 mV). The integration of Ni_xFe_yP, LDH and GO could endow these flower-like products with efficient activity. Although the Ni_xFe_yP/ LDH/GO heterojunction performed well in the HER catalysis process, as the same time, their OER electrocatalytic activity was measured. IrO_2 was selected as the precious metal-based comparison sample. It was observed from Figure 3d and Figure S8 that Ni foam and LDH/GO

DOI: 10.14102/j.cnki.0254-5861.2022-0048

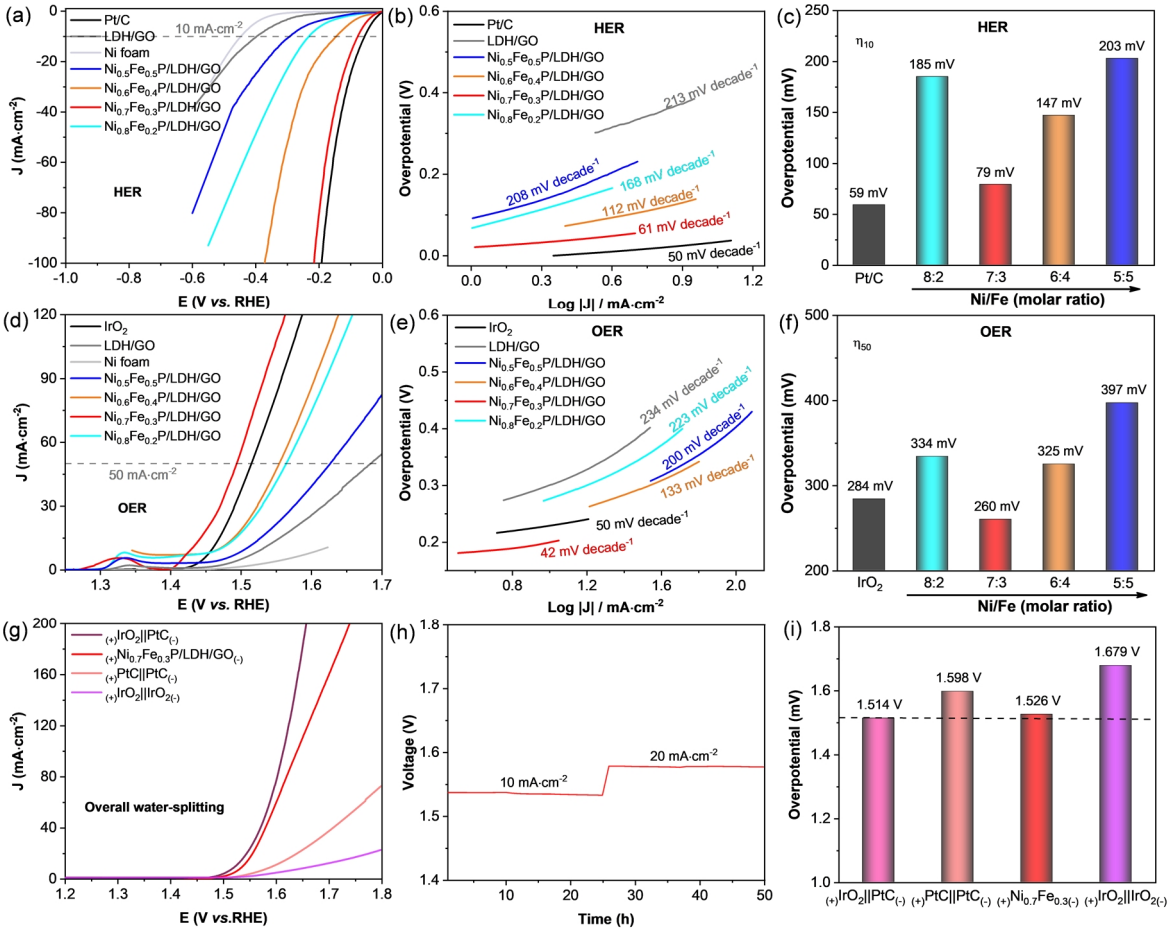

Figure 3. (a–c) The electrochemical properties of HER in 1 M KOH: (a) Polarization curves of Ni_xFe_yP/LDH/GO with different Ni/Fe molar ratio, LDH/GO and Pt/C, (b) The corresponding Tafel plots, (c) The corresponding overpotential values at J = 10 mA·cm^{-2}. (d–f) The electrochemical properties of OER in 1 M KOH: (d) Polarization curves of Ni_xFe_yP/LDH/GO with different Ni/Fe molar ratios, LDH/GO and IrO_2, (e) The corresponding Tafel slopes, (f) The corresponding overpotential values at J = 50 mA·cm^{-2}. (g–i) Electrolyzer performance for overall water splitting: (g) Polarization curves ($_{(-)}$ represents cathode, $_{(+)}$ represents anode), (h) Galvanostatic test curves of the $Ni_{0.7}Fe_{0.3}P$/LDH/GO, (i) Comparison of the cell voltages to achieve 10 mA·cm^{-2} among different electrolyzers in 1 M KOH.

had relatively negligible catalytic activity, while the Ni_xFe_yP/LDH/GO heterojunction required a lower overpotential. $Ni_{0.7}Fe_{0.3}P$/LDH/GO only required an overpotential of 198 mV at 10 mA·cm^{-2} (260 mV at 50 mA·cm^{-2}). Tafel slope and overpotential of all samples (Figure 3e–f) were considered together, and the results showed that the $Ni_{0.7}Fe_{0.3}P$/LDH/GO heterojunction had excellent catalytic performance. These results are in accordance with that of the HER performance, which also proved that the $Ni_{0.7}Fe_{0.3}P$/LDH/GO heterojunction had excellent dual-functional catalytic properties.[42] Furthermore, electrochemical HER/OER stability tests were performed via constant current and constant voltage tests, respectively. After stability test, the HER and OER performance was almost unchanged, as Figure S9 shows.

Driven by the outstanding dual-functional (HER and OER) electrocatalytic performance, an electrolyzer was assembled to achieve overall water-splitting. As shown in Figure 3g, $Ni_{0.7}Fe_{0.3}P$/LDH/GO was used as both anode and cathode. The noble metal-based electrocatalysts were used as controls and tested under the same conditions. $Ni_{0.7}Fe_{0.3}P$/LDH/GO exhibited a comparable activity to that of precious metal-based catalysts. As an evidence, the water splitting voltage of 1.526 V at 10 mA·cm^{-2} was sufficient against the reported catalysts, the reported catalysts, such as CoP (E_{10} = 1.65 V)[43], Fe_2O_3 and FeF_2 (E_{10} = 1.58 V)[44], MoO_2@ MoS_2@ Co_8S_9 (E_{10} = 1.62 V)[45]. This cost-effective feature and long-term stability enable $Ni_{0.7}Fe_{0.3}P$/LDH/GO to achieve continuous hydrogen production at 10 and 20 mA·cm^{-2}, as depicted in Figure 3h. Meanwhile, comparing the material structure and element chemical state before and after overall water splitting (Figure S10–12) showed that the heterojunction composition and structure had slight changes, which also proved that the catalyst oxidation is inevitable during the reaction process. To verify its hydrogen production efficiency, it is assumed that the theoretical Faraday efficiency of HER and OER is 100%. A large number of bubbles continue to overflow from near the electrodes of the electrolyzer, which also proves that the heterojunction material is continuously and stably catalyzing the water splitting process. By using a gas chromatograph, the actual hydrogen and oxygen production are obtained in Figure S13, and then FE ≈ 98% was cal-

DOI: 10.14102/j.cnki.0254-5861.2022-0048

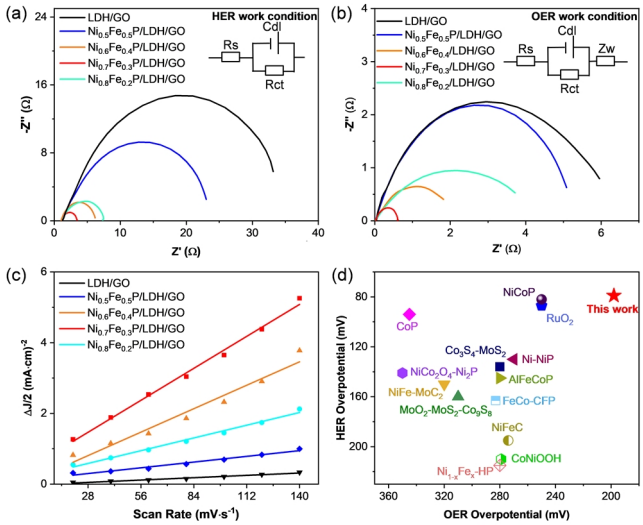

Figure 4. (a) EIS Nyquist plots for the HER in 1 M KOH, (b) EIS Nyquist plots for the OER in 1 M KOH, (c) Obtained correspondent C_{dl}, (d) Overall water splitting performance of $Ni_{0.7}Fe_{0.3}P$/LDH/GO compared with reported catalysts (HER and OER overpotential at 10 mA·cm^{-2}).

culated.

To assess the kinetic behavior of the catalysts, electrochemical impedance spectroscopy (EIS) is performed both under HER and OER work conditions (Figure 4a–b). With minimal semicircle obtained, $Ni_{0.7}Fe_{0.3}P$/LDH/GO exhibits the smallest charge transfer resistance and thus the best charge transfer ability in all as-prepared samples. Meanwhile, a lower Tafel slope of catalyst also proves the fast kinetics of $Ni_{0.7}Fe_{0.3}P$/LDH/GO. According to the Raman spectroscopy results (Figure S14), this new type of bimetal-induced heterojunction connected with GO has a high degree of graphitized carbon.[46] Specifically, the intensity of the D peak (1300 cm^{-1}) is equal to that of the G peak (1580 cm^{-1}), which facilitates the smooth conduction of electrons in the electrocatalytic process, thereby reducing the reaction kinetic barrier.[47,48] To assess the ECSA of the as-prepared catalysts, CV measurement with various scan rates (20, 40, 60, etc. mV·s^{-1}) was proceeded to obtain a series of values of the double layer capacitance (C_{dl}).[42] Based on CV results shown in Figure S15 and 4c, varied values of C_{dl}, 12.8, 32.3, 23.7, 5.8 and 2.4 mF·cm^{-2} have been received, corresponding to $Ni_{0.8}Fe_{0.2}P$/LDH/GO, $Ni_{0.7}Fe_{0.3}P$/LDH/GO, $Ni_{0.6}Fe_{0.4}P$/LDH/GO, $Ni_{0.5}Fe_{0.5}$/LDH/GO and LDH/GO, demonstrating the electrochemically active surface area (ECSA) of 0.32, 0.8075, 0.5925, 0.145 and 0.06 cm^2, respectively. Obviously, when the Ni/Fe molar ratio is 7:3, the ECSA of catalyst is by far the largest. The nitrogen adsorption- desorption test (Figure S16) further proved that the heterogeneous structure has a larger specific surface area (186.6 m^2·g^{-1}). During the in-situ phosphating process, a part of the NiFe LDH loses -OH or CO_3^{2-}, which can cause porous characteristics in catalysts morphology.[49] This porous structure can support full contact between the electrolyte and the catalyst, facilitating mass transfer and products releasing.[50] Based on the above merits, $Ni_{0.7}Fe_{0.3}P$/LDH/GO achieved excellent bi-functional performance, even better than that of the commercial RuO_2 and most of the reported transition metal based OER electrocatalysts (Figure 4d).

n CONCLUSION

In summary, we developed a method of introducing intense active sites into catalysts by constructing abundant interfaces at nanoscale. A series of bimetal-induced heterojunctions construc ted with Ni–Fe phosphide, LDH, and GO through hydrothermal reaction and subsequent phosphatization was fabricated and their HER and OER performance were studied. The optimized $Ni_{0.7}Fe_{0.3}P$/LDH/GO possesses a ECSA of one magnitude higher than LDH/GO. Favored by this, when applied to the water splitting electrolyzer, $Ni_{0.7}Fe_{0.3}P$/LDH/GO exhibited an ultra-low water splitting voltage with 1.526 and 1.546 V at 10 and 20 mA·cm^{-2}, respectively. This work provides a new strategy to obtain low-cost and reliable heterojunction-based electrocatalysts.

n EXPERIMENTAL

Material and Reagents. Graphite powder, sodium nitrate, potassium permanganate, nickel(II) nitrate hexahydrate, ferric(III) nitrate nonahydrate ($Fe(NO_3)_3·9H_2O$, 98%), urea (CH_4NO_2, 99.5%), Ni foam (NF 1×1 cm^2), trisodium citrate dehydrate ($Na_3C_6H_5O_7·2H_2O$, 99%), nitric acid (HNO_3, 70%) and sulfuric acid (H_2SO_4, 98%). All reagents were purchased from Chengdu Kelong Chemical Reagent Factory and used without further purification.

Synthesis of Graphene Oxide. GO was synthesized by the modified Hummers method.[26] 1 g graphite and 0.5 g $NaNO_3$ were separately poured into concentrated H_2SO_4 (100 mL, 98%) under vigorous stirring. After 30 min, 6 g $KMnO_4$ was added gradually with an ice bath, which kept the temperature below 20 ℃. Then the mixture was magnetically stirred at 40 ℃ for 12 hours. 200 mL H_2O was dripped to the pasty mixture for dilution. Subsequently, 1 mL 30% H_2O_2 was added. Finally, the diluted solution was washed and dried at 60 ℃ overnight.

Synthesis of Ni_xFe_y/LDH/GO. In this step, Ni_xFe_y/LDH/GO with different molar ratios of Ni and Fe was prepared. For a typical synthesis of $Ni_{0.7}Fe_{0.3}$, 0.72 g $Ni(NO_3)_2·6H_2O$, 0.17 g urea, 0.33 g $Fe(NO_3)_3·9H_2O$, 0.08 g $Na_3C_6H_5O_7·2H_2O$ and 20 mL GO (100 mg/mL) were dissolved in 105 mL deionized water under magnetic stirring. After 10 min, the mix liquor was poured into three 50 mL Teflon-lined stainless-steel autoclaves and reacted at 180 ℃ for 8 hours. Then, the products were washed and dried at 70 ℃ for 6 hours. The precursors with different Ni/Fe rations of Ni_xFe_y/LDH/GO were obtained via adjusting the molar ratios of Ni/Fe (8:2, 6:4 and 5:5) of dissolved Ni/Fe source and the others were the same as the above process. For simplicity, $Ni_{0.7}Fe_{0.3}$/LDH/GO is denoted as LDH/GO unless otherwise stated.

Synthesis of Ni_xFe_yP/LDH/GO. To prepare Ni_xFe_yP/LDH/GO, 100 mg Ni_xFe_y/LDH/GO and 500 mg $NaH_2PO_2·H_2O$ were placed on both ends of the graphite boat, respectively, which was sealed completely with a lid. Afterward, the graphite boat was put into a tubular furnace filled. After argon flow was lasted for 30 min, the flat-temperature of the tubular furnace was heated from room temperature to 300 ℃ at a ramp of 2 ℃·min^{-1}, and then continued keeping 300 ℃ for 1 hour. Finally, the products were gradually

DOI: 10.14102/j.cnki.0254-5861.2022-0048

cooled to natural temperature.

Preparation of 20 wt% Pt/C@NF and IrO_2@NF. For comparison of the H_2 and O_2 generation activity for both HER and OER, 5 mg Pt/C or IrO_2 (20 wt%) was dispersed in a mixed liquor including 100 μL Nafion (0.5 wt%) and 200 μL ethanol by ultrasound. After 1 hour, the as-prepared suspension solution was homogeneously dipped on NF (1 x 1 cm^2) and dried naturally. The Ni_xFe_yP/LDH/GO/NF, NiFe LDH/GO/NF and NF were prepared with the same method.

Materials Characterization. All phase analyses of samples were characterized by X-ray diffraction (XRD, PANalytical X'Pert Powder). Field emission scanning electron microscopy (SEM, JEOL JSM-7800F) and energy-dispersive X-ray spectrum analysis (EDS) were used to investigate the morphologies and element mapping of samples. The structural features and element distribution of synthesized catalysts were collected by a FEI talos transmission electron microscope with an accelerate voltage of 200 kV. Element valence was recorded using X-ray photoelectron spectroscopy (XPS, Thermo Fisher Scientific ESCALAB250Xi) with the binding energy of C1*s* calibrated into 284.8 eV. Raman spectra were performed on a LabRAM HR Evolution with a 532 nm laser at ambient temperature. Thermogravimetry (TG, TGA/DSC1/1600LF) was recorded on the phase transition of products and the surface area and pore size were detected by nitrogen adsorption-desorption analysis (Quantachrometer Autosorb-6B). Inductively coupled plasma emission spectrometry (ICP-MS, Plasma 1000) was carried out to explore the elemental contents of electrocatalysts.

Electrochemical Measurements. HER and OER were tested by an electrochemical workstation (CHI660E, Shanghai) with a three-electrode system (Ni_xFe_yP/LDH/GO/NF as working electrode, Au as counter electrode, Hg/HgO as reference electrode). Overall water splitting used a traditional two-electrode system electrochemical workstation ($Ni_{0.72}Fe_{0.33}P$/LDH/GO/NF as both anode and cathode). To obtain the polarization curves, linear sweep voltammetry (LSV) with a scan rate of 5 $mV \cdot s^{-1}$ in 1 M KOH was performed for the HER and OER (E(RHE) = E(Hg/HgO) + 0.098 + 0.059 pH). Briefly, for evaluating the ECSA, cyclic voltammetry (CV) was used between 0.18 to 0.28 V vs. RHE at various scan rates from 20 to 140 $mV \cdot s^{-1}$. Electrochemical impedance spectroscopy (EIS) and constant current and constant voltage tests were carried out for the stability and durability of electrocatalysis. Finally, the Faraday efficiency (FE) was estimated by a gas chromatograph.

$$EF = \frac{V_{(measured)}}{V_{(calculated)}} = \frac{v(mesured)/v_m}{\frac{Q}{nF}}$$

Where V_m represents the molar volume of gas under 24.5 $L \cdot mol^{-1}$, 298 K, 101 KPa, Q is the charge passing through the electrode, n is n moles of electrons per mole of gas, and F means the Faraday constant (96485 $C \cdot mol^{-1}$).

n ACKNOWLEDGEMENTS

The authors acknowledge the financial support from the National Key Research and Development Program of China (2019YFC0214402). They also thank Prof. B. Zhang from Analytical & Testing Center of Chongqing University for TEM characterization.

n AUTHOR INFORMATION

Corresponding authors. Emails: 18811419320@163.com and lzq0313@cqu.edu.cn

n COMPETING INTERESTS

The authors declare no competing interests.

n ADDITIONAL INFORMATION

Supplementary information is available for this paper at http://manu30.magtech.com.cn/jghx/EN/10.14102/j.cnki.0254-5861.2022-0048

For submission: https://mc03.manuscriptcentral.com/cjsc

n REFERENCES

(1) Linkous, D.; Muradov, L. Sustainable hydrogen production. *Science* **1996**, 305, 972–974.

(2) Yin, H. J.; Zhao, S. L.; Zhao, K.; Muqsit, A.; Tang, H. J.; Chang, L.; Zhao, H. J.; Gao, Y.; Tan, Z. Y. Ultrathin platinum nanowires grown on single-layered nickel hydroxide with high hydrogen evolution activity. *Nat. Commun*. **2015**, 6, 6430.

(3) Cheng, N. C.; Stambula, S.; Wang, D.; Banis, M. N.; Liu, J.; Riese, A.; Xiao, B. W.; Li, R. Y.; Sham, T. K.; Liu, L. M.; Botton, G. A.; Sun, X. L. Platinum single-atom and cluster catalysis of the hydrogen evolution reaction. *Nat. Commun*. **2016**, 7, 13638.

(4) Gür, T. M. Critical review of carbon conversion in "carbon fuel cells". *Chem. Rev*. **2013**, 113, 6179–6206.

(5) Zhi, W. S.; Jakob, K.; Colin, F. D.; Chorkendorff, I.; Nørskov, J. K.; Jaramillo, T. F. Combining theory and experiment in electrocatalysis: insights into materials design. *Science* **2017**, 355, 1-14.

(6) Shi, Q. R.; Zhu, C. Z.; Du, D.; Lin, Y. H. Robust noble metal-based electrocatalysts for oxygen evolution reaction. *Chem. Soc. Rev*. **2019**, 48, 3181–3192.

(7) Shinagawa, T.; Takanabe, K. Towards versatile and sustainable hydrogen production through electrocatalytic water splitting: electrolyte engineering. *ChemsSusChem*. **2017**, 10, 1318–1336.

(8) Zhao, H. Y.; Wang, Y. W.; Fang, L.; Fu, W. W.; Yang, X. H.; You, S. L.; Luo, P.; Zhang, H. J.; Wang, Y. Cation-tunable flower-like (Ni_xFe_{1-x})2P@graphitized carbon films as ultrastable electrocatalysts for overall water splitting in alkaline media. *J. Mater. Chem. A* **2019**, 7, 20357–20368.

(9) Anantharaj, S.; Ede, S. R.; Sakthikumar, K.; Karthick, K.; Mishra, S.; Kundu, S. Recent trends and perspectives in electrochemical water splitting with an emphasis on sulfide, selenide, and phosphide catalysts of Fe, Co, and Ni: a review. *ACS Catal.* **2016**, 6, 8069–8097.

(10) Bai, Y. J.; Zhang, H. J.; Li, X.; Liu, L.; Xu, H. T.; Qiu, H. J.; Wang, Y. Novel peapod-like Ni_2P nanoparticles with improved electrochemical properties for hydrogen evolution and lithium storage. *Nanoscale* **2015**, 7, 1446–1453.

(11) Deng, B.; Zhou, L. S.; Jiang, C. Q.; Jiang, Z. J. High catalytic performance of nickel foam supported Co_2P-Ni_2P for overall water splitting and its structural evolutions during hydrogen/oxygen evolution reactions in alkaline solutions. *J. Catal*. **2019**, 373, 81–92.

(12) Liu, M.; Yang, L. M.; Liu, T.; Tang, Y. H.; Luo, S. L.; Liu, C. B.; Zeng,

DOI: 10.14102/j.cnki.0254-5861.2022-0048

Y. X. Fe_2P/reduced graphene oxide/Fe_2P sandwich structured nanowall arrays: a high-performance non-noble-metal electrocatalyst for hydrogen evolution. *J. Mater. Chem. A* **2017**, 5, 8608–8615.
(13) Shi, Y. M.; Zhang, B. Recent advances in transition metal phosphide nanomaterials: synthesis and applications in hydrogen evolution reaction. *Chem. Soc. Rev*. **2016**, 45, 1529–1541.
(14) Xu, Y. L.; Wang, C.; Huang, Y. H.; Fu, J. Recent advances in electrocatalysts for neutral and large-current-density water electrolysis. *Nano Energy* **2021**, 80, 105545.
(15) Liang, H. F.; Gandi, A. N.; Xia, C.; Hedhili, M. N.; Anjum, D. H.; Schwingenschlögl, U.; Alshareef, H. N. Amorphous NiFe-OH/NiFeP electrocatalyst fabricated at low temperature for water oxidation applications. *ACS. Energy Lett*. **2017**, 2, 1035–1042.
(16) Zhang, B. W.; Lui, Y. H.; Ni, H. W.; Hua, S. Bimetallic $(Fe_xNi_{i1-x})_2P$ nanoarrays as exccptionally efficient electrocatalysts for oxygen evolution in alkaline and neutral media. *Nano Energy* **2017**, 38, 553–560.
(17) Hou, Y.; Lohe, M. R.; Zhang, J.; Liu, S. H.; Zhuang, X. D.; Feng, X. L. Vertically oriented cobalt selenide/NiFe layered-double-hydroxide nanosheets supported on exfoliated graphene foil: an efficient 3D electrode for overall water splitting. *Energy Environ. Sci.* **2016**, 9, 478–483.
(18) Jia, W. Y.; Zhang, L.; Gao, G.; Chen, H.; Wang, B.; Zhou, J.; Soo, M. T.; Hong, M.; Yan, X.; Qian, G.; Zou, J.; Du, A.; Yao, X. A heterostructure coupling of exfoliated Ni–Fe Hydroxide nanosheet and defective graphene as a bifunctional electrocatalyst for overall water splitting. *Adv. Mater*. **2017**, 29, 1230–1235.
(19) Liu, T.; Li, A.; Wang, C.; Zhou, W.; Liu, S.; Guo, L. Interfacial electron transfer of Ni_2P-NiP_2 polymorphs inducing enhanced electrochemical properties. *Adv. Mater.* **2018**, 30, e1803590.
(20) Feng, J. X.; Ye, S. H.; Xu, H.; Tong, Y. X.; Li, G. R. Design and synthesis of FeOOH/CeO_2 heterolayered nanotube electrocatalysts for the oxygen evolution reaction. *Adv. Mater.* **2016**, 28, 4698–4703.
(21) Li, M.; Fang, L. G. $NiSe_2$-$CoSe_2$ with a hybrid nanorods and nanoparticles structure for efficient oxygen evolution reaction. *Chin. J. Struct. Chem*. **2022**, 41, 2201019–2201024.
(22) Huang, C.; Miao, X.; Pi, C.; Gao, B.; Zhang, X.; Qin, P.; Huo, K.; Peng, X.; Chu, P. K. Mo_2C/VC heterojunction embedded in graphitic carbon network: an advanced electrocatalyst for hydrogen evolution. *Nano. Energy* **2019**, 60, 520–526.
(23) Gao, Y.; Lang, Z.; Yu, F.; Tan, H.; Yan, G.; Wang, Y.; Ma, Y.; Li, Y. A Co_2P/WC nano-heterojunction covered by N-doped carbon as high efficient electrocatalyst for hydrogen evolution reaction. *Chemsuschem*. **2018**, 11, 1082–1091.
(24) Ledendecker, M.; Calderon, S. K.; Papp, C.; Steinruck, H. P.; Antonietti, M.; Shalom, M. The synthesis of nanostructured Ni_5P_4 films and their use as a non-noble bifunctional electrocatalyst for full water splitting. *Angew. Chem. Int. Ed.* **2015**, 54, 12361–12365.
(25) Zhang, G.; Wang, G.; Liu, Y.; Liu, H.; Qu, J.; Li, J. Highly active and stable catalysts of phytic acid-derivative transition metal phosphides for full water splitting. *J. Am. Chem. Soc.* **2016**, 138, 14686–14693.
(26) Cui, Y. Q.; Xu, J. X.; Wang, M. L.; Guan, L. H. Surface oxidation of single-walled-carbon-nanotubes with enhanced oxygen electroreduction activity and selectivity. *Chin. J. Struct. Chem*. **2021**, 5, 533–539.
(27) Hummers W, O. R. Preparation of graphitic oxide. *J. Am. Chem. Soc.* **1985**, 80, 1339.
(28) Popczun, E. J.; McKone, J. R.; Read, C. G.; Biacchi, A. J.; Wiltrout, A. M.; Lewis, N. S.; Schaak, R. E. Nanostructured nickel phosphide as an electrocatalyst for the hydrogen evolution reaction. *J. Am. Chem. Soc.* **2013**, 135, 9267–9270.
(29) Chen, S.; Yu, C.; Cao, Z. F.; Huang, X. P.; Wang, S.; Zhong, H. Trimetallic NiFeCr-LDH/MoS_2 composites as novel electrocatalyst for OER. *Int. J. Hydrogen Energy* **2020**, 46, 7037–7046.
(30) Moon, J. S.; Jang, J. L.; Kim, E. G.; Chuang, Y. H.; Yoo, S. J.; Lee, Y. K. The nature of active sites of Ni_2P electrocatalyst for hydrogen evolution reaction. *J. Catal.* **2015**, 326, 92–99.
(31) Stern, L. A.; Feng, L.; Song, F.; Hu, X. Ni_2P as a Janus catalyst for water splitting: the oxygen evolution activity of Ni_2P nanoparticles. *Energy Environ. Sci.* **2015**, 8, 2347–2351.
(32) Ledendecker, M.; Krick Calderón, S.; Papp, C.; Steinrück, H. P.; Antonietti, M.; Shalom, M. The synthesis of nanostructured Ni_5P_4 films and their use as a non-noble bifunctional electrocatalyst for full water splitting. *Angew. Chem. Int. Ed.* **2015**, 54, 12361–12365.
(33) Liu, P. F.; Li, X.; Yang, S.; Zu, M. Y.; Liu, P.; Zhang, B.; Zheng, L. R.; Zhao, H.; Yang, H. G. $Ni_2P(O)$/$Fe_2P(O)$ interface can boost oxygen evolution electrocatalysis. *ACS Energy Lett.* **2017**, 2, 2257–2263.
(34) Tang, C.; Zhang, R.; Lu, W.; He, L.; Jiang, X.; Asiri, A. M.; Sun, X. Fe-doped CoP nanoarray: a monolithic multifunctional catalyst for highly efficient hydrogen generation. *Adv. Mater.* **2017**, 29, 1602441.
(35) Zhang, B.; Lui, Y. H.; Ni, H.; Hu, S. Bimetallic $(Fe_xNi_{i1-x})_2P$ nanoarrays as exceptionally efficient electrocatalysts for oxygen evolution in alkaline and neutral media. *Nano Energy* **2017**, 38, 553–560.
(36) Zheng, J.; Zhou, W.; Liu, T.; Liu, S.; Wang, C.; Guo, L. Homologous NiO/Ni_2P nanoarrays grown on nickel foams: a well matched electrode pair with high stability in overall water splitting. *Nanoscale* **2017**, 9, 4409–4418.
(37) Hou, Y.; Lohe, M. R.; Zhang, J.; Liu, S.; Zhuang, X.; Feng, X. Vertically oriented cobalt selenide/NiFe layered-double-hydroxide nanosheets supported on exfoliated graphene foil: an efficient 3D electrode for overall water splitting. *Energy Environ. Sci.* **2016**, 9, 478–483.
(38) Asnavandi, M.; Zhao, C. Autologous growth of nickel oxyhydroxides with in situ electrochemical iron doping for efficient oxygen evolution reactions. *Mater. Chem. Front.* **2017**, 1, 2541–2546.
(39) Konkena, B.; Masa, J.; Botz, A. J. R.; Sinev, I.; Xia, W.; Koßmann, J.; Drautz, R.; Muhler, M.; Schuhmann, W. Metallic $NiPS_3$@NiOOH core-shell heterostructures as highly efficient and stable electrocatalyst for the oxygen evolution reaction. *ACS Catal.* **2016**, 7, 229–237.
(40) Lu, Y.; Wang, X.; Mai, Y.; Xiang, J.; Zhang, H.; Li, L.; Gu, G.; Tu, T.; Mao, S. X. Ni_2P/Graphene sheets as anode materials with enhanced electrochemical properties versus lithium. *J. Phys. Chem. C* **2012**, 116, 22217–22225.
(41) Jiang, B.; Jing, C.; Yuan, Y.; Feng, L.; Liu, L.; Dong, F.; Dong, B.; Zhang, Y. X. 2D-2D growth of NiFe LDH nanoflakes on montmorillonite for cationic and anionic dye adsorption performance. *J. Colloid Interface Sci.* **2019**, 540, 398–409.
(42) Song, B.; Li, K.; Yin, Y.; Wu, T.; Dang, L.; Cabán-Acevedo, M.; Han, J.; Gao, T.; Wang, X.; Zhang, Z.; Schmidt, J. R.; Xu, P.; Jin, S. Tuning mixed nickel iron phosphosulfide nanosheet electrocatalysts for enhanced hydrogen and oxygen evolution. *ACS Catal.* **2017**, 7, 8549–8557.
(43) Liu, T.; Xie, L.; Yang, J.; Kong, R.; Du, G.; Asiri, A. M.; Sun, X.; Chen, L. Self-standing cop nanosheets array: a three-dimensional bifunctional catalyst electrode for overall water splitting in both neutral and alkaline Media. *ChemElectroChem*. **2017**, 4, 1840–1845.
(44) Fan, X.; Liu, Y.; Chen, S.; Shi, J.; Wang, J.; Fan, A.; Zan, W.; Li, S.; Goddard, W. A.; Zhang, X. M. Defect-enriched iron fluoride-oxide nano-

DOI: 10.14102/j.cnki.0254-5861.2022-0048

porous thin films bifunctional catalyst for water splitting. *Nat Commun*. **2018**, 9, 1809.
(45) Li, Y.; Wang, C.; Cui, M.; Xiong, J.; Mi, L.; Chen, S. Heterostructured MoO_2@MoS_2@Co_9S_8 nanorods as high efficiency bifunctional electrocatalyst for overall water splitting. *Appl. Surf. Sci*. **2021**, 543, 148804.
(46) Joya, K. S.; Sala, X. *In situ* Raman and surface-enhanced Raman spectroscopy on working electrodes: spectroelectrochemical characterization of water oxidation electrocatalysts. *Phys. Chem. Chem. Phys.* **2015**, 17, 21094–21103.
(47) Eckmann, A.; Felten, A.; Mishchenko, A.; Britnell, L.; Krupke, R.; Novoselov, K. S.; Casiraghi, C. Probing the nature of defects in graphene by Raman spectroscopy. *Nano Lett.* **2012**, 12, 3925–3930.
(48) Liu, M.; Gan, L.; Xiong, W.; Xu, Z.; Zhu, D.; Chen, L. Development of MnO_2/porous carbon microspheres with a partially graphitic structure for high performance supercapacitor electrodes. *J. Mater. Chem. A* **2014**, 2, 2555–2562.
(49) Zhou, Y.; Wang, Y.; Zhao, H.; Su, J.; Zhang, H.; Wang, Y. Investigation of anion doping effect to boost overall water splitting. *J. Catal.* **2020**, 381, 84–95.
(50) Wang, H.; Wang, Y.; Tan, L.; Fang, L.; Yang, X.; Huang, Z.; Li, J.; Zhang, H.; Wang, Y. Component-controllable cobalt telluride nanoparticles encapsulated in nitrogen-doped carbon frameworks for efficient hydrogen evolution in alkaline conditions. *Appl. Catal. B* **2019**, 244, 568–575.

Received: March 2, 2022
Accepted: April 2, 2022
Published: April 8, 2022

DOI: 10.14102/j.cnki.0254-5861.2022-0048